Hall effect of as-grown oxygen-deficient $YBa_2Cu_3O_x$ thin films

M. S. Raven and Y. M. Wan
Department of Electrical and Electronic Engineering, University of Nottingham, Nottingham NG7 2RD, England
(Received 5 August 1994; revised manuscript received 5 October 1994)

The resistivity and Hall effect have been measured in a number of samples of *as-grown*, oxygen deficient, *c*-axis-oriented $YBa_2Cu_3O_x$ thin films, both as a function of temperature and oxidation state. The temperature dependence of the longitudinal resistivity and Hall coefficient were generally similar to films prepared by *ex-situ* oxidation processes with the R-T and $1/R_H$-T characteristics nearly linear and $\cot\theta_H \propto T^2$. Small deviations from these laws were investigated and a quadratic fit obtained for the resistivity data and a cubic fit for $\cot\theta_H$ but with dominant linear and quadratic terms, respectively. From the empirical data, expressions for the effective carrier relaxation times and mobilities were obtained and compared with other possible scattering mechanisms. In contrast to films reoxidized after growth, we find that for the as-grown films the Hall mobility μ_H increases sharply and $\cot\theta_H$ decreases with increasing oxygen content. This is discussed in terms of different oxidation conditions that lead to different lattice defects for the two cases.

I. INTRODUCTION

The Hall effect provides a powerful experimental technique when applied to superconductors, both for the normal state and superconducting state, yielding the carrier type, carrier density, mobility, and scattering characteristics. Soon after the discovery of high-temperature superconductors (HTS's), Hall effect measurements were obtained and anomalous effects reported both for the normal state[1] and the superconducting–normal-state transition region.[2] These measurements yielded the well-known results that in the normal state the free carriers in $YBa_2Cu_3O_x$ (YBCO) are holelike. The anisotropic resistivity decreases nearly linearly with decreasing temperature for transport in the *ab* plane of the YBCO unit cell but increases semiconductorlike for transport in the *c* direction.[3–5] The inverse Hall coefficient or Hall density decreases nearly linearly with decreasing temperature, increases sharply near T_c, changes sign, and then decreases to zero. The ratio of the transverse voltage to longitudinal voltage is proportional to the Hall tangent and its inverse, $\cot\theta_H$, provides a direct measure of the carrier scattering rate. The dependence of $\cot\theta_H$ on sample properties and the implications for HTS's are of considerable interest both theoretically and experimentally.[6–9]

The Hall effect has been investigated using various forms of YBCO material including sintered polycrystalline ceramics,[1,2,10–19] bulk single crystals,[20–25] and *c*-axis-oriented thin films.[26–31] These investigations include the effects of oxygen deficiency and doping with nonmagnetic[15–17,24] and magnetic impurities.[18,19,25] This has created an extensive field of research, particularly if all the different HTS cuprates are included. In this paper, attention is focused on "as-grown" oxygen-deficient *c*-axis YBCO thin films. In much of the work to date on oxygen deficiency, the oxidation procedure has taken place *after* film deposition in controlled diffusion experiments. The advantage of this procedure is that only a single specimen is used under various oxidation states so that differences between specimens is avoided. However, the oxygen diffusion coefficient is low along the *c*-axis ($\approx 10^{-12}$ cm^2 s^{-1}), and the final oxidation state of the film depends on the diffusion mechanism. This may be different for as-grown material compared with material that has been oxidized in separate experiments. We have therefore undertaken a Hall-effect investigation using a number of oxygen-deficient YBCO films prepared *in situ* in the deposition chamber. This has meant carrying out measurements on different samples, so particular care was taken in sample characterization. In particular, detailed x-ray-diffraction measurements were made in order to identify any *a*-axis material, which can have a significant effect on transport characteristics. Although the use of separate samples may cause problems in the determination of absolute values of resistivity and Hall coefficient, errors are reduced in the calculation of the Hall angle, $\cot\theta_H$, and mobility, since these depend on the ratio of the resistivity and Hall coefficient. Errors due to common geometrical factors such as the film thickness are reduced. Oxygen-deficient films also show deviations from linear resistivity-temperature behavior, even for oriented *c*-axis or single-crystal material. We have therefore found the best-fit expressions for both the resistivity and Hall coefficient and obtained an equation for $\cot\theta_H$ from which different scattering mechanisms were identified.

II. EXPERIMENTAL TECHNIQUES

The YBCO thin films were produced by *in situ*, off-axis, rf magnetron sputter deposition from a single compound YBCO target. Further details about the sputtering system and techniques used are given in Refs. 32 and 33. The substrates were mainly 10-mm-square, 1-mm-thick optically polished single-crystal (100)-oriented MgO. Prior to deposition the substrates received a stan-

dard solvent cleaning procedure, finally rinsing in distilled water before mounting on a YBCO-coated stainless steel substrate heater.[34] The substrates were bonded to the heater using silver foil or silver paint. Substrate temperatures were measured using a Chromel-Alumel (type-*K*) thermocouple spot welded to the heater plate adjacent to the substrates. This temperature measurement was checked in a separate experiment by bonding a second thermocouple to the substrate surface. This indicated a temperature about 10 °C lower than the thermocouple next to the substrate. The sputtering system had a base pressure of less than 2×10^{-6} Torr and deposition was carried out with Ar/O_r 4:1, total pressure 280 mTorr (20% or 56 mTorr of oxygen), substrate temperature between 690 and 735 °C, and typical growth rates of 0.4 nm/min. At the end of the deposition period the argon gas was turned off and the oxygen pressure increased to between 1 and 2 Torr. The substrate temperature was then decreased to 425–475 °C, and the film annealed in oxygen for 1 h, after which the heater was switched off and the film allowed to cool to room temperature. This procedure led to oxygen-deficient films *as grown* and without the need to carry out separate oxygenation and annealing experiments.

The crystal structure of the films was determined by x-ray diffractometry (XRD) and a typical XRD trace for YBCO sputtered on MgO(100) is shown in Fig. 1. Apart from substrate peaks this shows only YBCO (00*l*) reflections. The large number of (00*l*) reflections allowed measurements of the *c*-axis lattice parameter to an error of less than 0.01 Å, sufficiently small to detect changes in *c* due to oxygen deficiency.[32] The oxygen content *x* was estimated from these lattice parameter measurements to an error of less than 0.1 using results given by Jorgensen *et al.*[35] and checked against critical temperature and resistivity measurements. Because of the small lattice mismatch of 2%, *a*-axis grains grow readily on $SrTiO_3$ (100) substrates. For growth on MgO (100) substrates the lattice mismatch is 9%, and *a*-axis growth is less probable. We have checked our films carefully for the presence of *a*-axis material using XRD, and for the samples reported here *a*-axis material was not detectable in the *c*-axis films on MgO (100) substrates. However, there was some suggestion of *a*-axis-oriented grains in the film-sputtered $SrTiO_3$ (100) substrate, sample No. Y116SP.

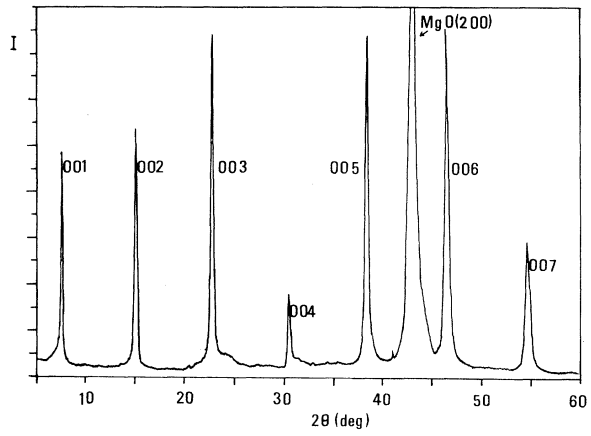

FIG. 1. X-ray-diffraction trace of $YBa_2Cu_3O_x$ sputtered onto MgO (100) showing *c*-axis alignment.

The thin-film Hall bar patterns were produced using wet etching and standard photolithography techniques.[36,37] The Hall bars consisted of a rectangular strip of YBCO with two pairs of sidearms. The strip width $w=1.2$ mm, distance between sidearms $l=2.2$ mm, and sidearm width $s=0.1$ mm. This latter width ensured that the sidearms had an insignificant effect on the equipotentials. This was checked using the expression[38]

$$V_{bb'}=V_{aa'}[1-p(a)w/(2l)] ,$$

where $V_{bb'}$ is the measured voltage between the sidearms, $V_{aa'}$ is the actual voltage, $a=[1+(w/s)^2]^{-1/2}$, and $p(a)$ is a function of a as given in Ref. 38. In our case $p\approx0$ and $V_{aa'}=V_{bb'}$. Film thicknesses were measured using a surface profile instrument scanning the stylus over the edges of the patterned films. Ohmic contacts were made by evaporating silver onto contact pads and bonding fine copper wires onto the silver pads with silver conducting paint. The normal-state resistivity measurements were performed using the standard four terminal technique by passing a constant current through the main body of the Hall bar and measuring the longitudinal voltage drop between sidearms. The Hall-effect measurements were made by measuring the transverse Hall voltage $V_y=V_H$ when a magnetic field B_z was applied perpendicular to the YBCO film with the film in the *x*-*y* plane and current flow in the *x* direction. The offset voltage due to the misalignment of the Hall electrodes was eliminated in the usual way by reversing the magnetic field and calculating the average value $V_H=[V_H(B^+)-V_H(B^-)]/2$.

III. EXPERIMENTAL RESULTS

The normalized resistivity, $\rho_n=\rho(T)/\rho_{300}$, versus temperature measurements for a number of samples is shown in Fig. 2. Although the graphs are quite linear over the

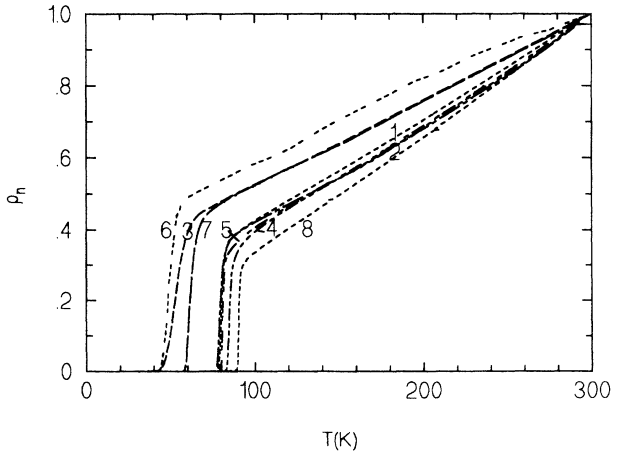

FIG. 2. Normalized resistivity, $\rho_n=\rho(T)/\rho_{300}$, versus temperature for a number of *c*-axis-oriented $YBa_2Cu_3O_x$ films. Oxygen levels are sample Nos. 6 and 3: $x=6.5$, 7: $x=6.46$, 1 and 2: $x=6.7$, 5: $x=6.8$, 4: $x=6.85$, and 8: $x\approx7$.

TABLE I. Critical temperatures measured at the midpoint of the transition, T_{cmid}, and the coefficients for the resistivity, Eq. (1), and inverse Hall coefficient, Eq. (3).

Device No.	T_{cmid} (K)	A ($\mu\Omega$ cm K^{-1})	B ($m\Omega$ cm K)	C ($\mu\Omega$ cm)	α (C cm^{-3} K^{-1})	R_{H0}^{-1} (C cm^{-3})
3. Y78MP	54	10.97	7.645	1183	1.76	158
2. Y113MP	79	0.951	5.203	−26.00	3.93	544
1. Y111MP	80	0.857	2.032	13.41	3.64	575
5. Y84MP	81	1.472	5.011	−8.85	1.86	176
4. Y116SP	85	1.278	4.156	−8.19	1.62	182

temperature range 100–300 K, they can be represented more accurately by the equation

$$\rho_{xx}=AT+B/T+C \quad (100\text{–}300\ \text{K}), \tag{1}$$

where the constants A, B, and C have been listed in Table I for a number of films. The resistivity values at 300 K in mΩ cm were sample (1) 0.276, (2) 0.28, (3) 4.5, (4) 0.39, and (5) 0.45. We note that although Eq. (1) is similar to that modeled for the resistivity of a film containing mixed c- and a-axis-oriented grains, in this case Eq. (1) arises from curve fitting, and the constants A, B, and C may not have the same significance.

The Hall coefficient R_H was determined from

$$R_H=V_y t/(B_z I), \tag{2}$$

where I is the longitudinal current, w the film width, and t the film thickness. The Hall voltage dependence on magnetic field and current was measured and found to be highly linear over a range 0–1 T and 0–20 mA. Figure 3 shows typical plots of both the Hall voltage V_H and $1/R_H$ versus temperature. The sign reversal of V_H at the superconducting transition was typical of the samples measured. The linearity of $1/R_H$ with T was also typical for the samples investigated, as shown in Fig. 4. This linear behavior deviated near T_c and also at temperatures near 300 K in some samples. However, for this limited temperature range the reciprocal Hall coefficient fitted the empirical equation

$$1/R_H=\alpha T+1/R_{H0} \quad (100\text{–}300\ \text{K}), \tag{3}$$

where α is the temperature coefficient of $1/R_H$ and $1/R_{H0}$ the extrapolated value of $1/R_H$ at $T=0$ K. Values of α and $1/R_{H0}$ were determined by least-squares and best-fit values are recorded in Table I. Using this data Fig. 5 shows plots of the Hall density, $n_H=1/(eR_H)$, and Hall density per unit cell $N_c=n_H V_c$, where e is the electronic charge and the unit-cell volume $V_c=0.172\times10^{-21}$ cm^{-3}.

The longitudinal and transverse voltage measurements yield directly the reciprocal Hall angle

$$\cot\theta_H=(V_x/V_y)w/l, \tag{4}$$

where w/l is the film width to length ratio as defined previously. Figure 6 shows plots of $\cot\theta_H$ versus T for the same set of samples. Above the transition region $\cot\theta_H$ increases monotonically with increasing temperature with some deviation occurring near room temperature. A large *increase* in $\cot\theta_H$ occurs for the film with the smallest x. Since $\cot\theta_H$ is proportional to the inverse relaxation time or directly proportional to the scattering rate, this suggests a higher density of scattering centers in this film. The values of $\cot\theta_H$ in Fig. 8 are considerably higher than values recently published.[30] This arises because $\cot\theta_H \propto 1/B$ [see Eq. (5)], and we have used $B=0.5$ and 0.74 T compared with typical values of 7 T used in recent work. We can also relate $\cot\theta_H$ to the empirical equations, (1) and (3), using

$$\cot\theta_H=\rho_{xx}/(R_H B_z). \tag{5}$$

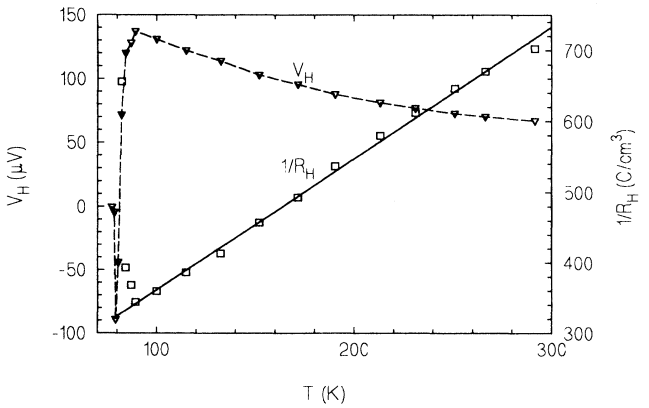

FIG. 3. Typical variation of V_H and $1/R_H$ with temperature (sample No. 5:Y84MP).

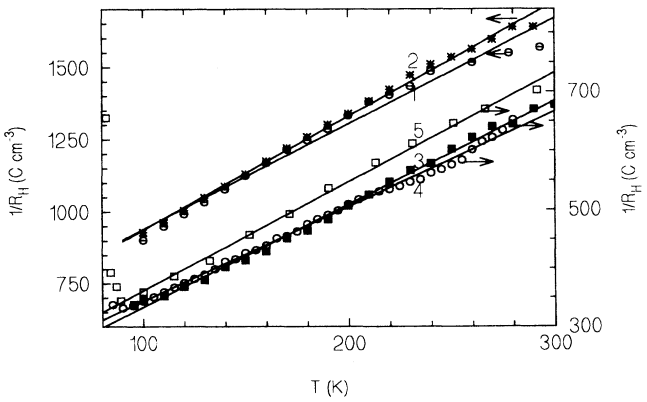

FIG. 4. Variation of $1/R_H$ with temperature for a number of samples. The straight lines fit Eq. (3) over the temperature range 100–300 K.

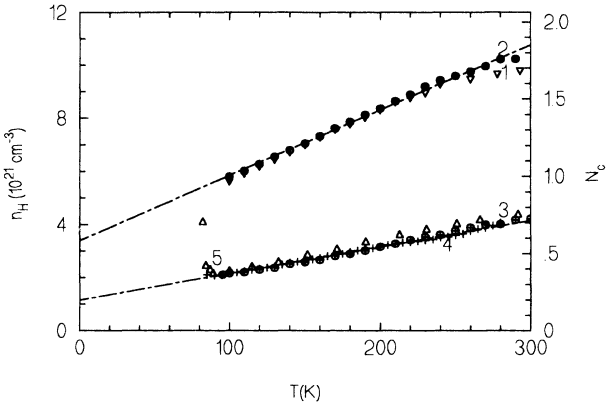

FIG. 5. Hall density n_H and unit-cell density N_c vs temperature for several samples.

The continuous curves in Fig. 6 are plots of Eq. (5) using the empirical expressions for ρ_{xx} and $1/R_H$ given by Eqs. (1) and (3), respectively. The excellent agreement between these curves and the data points is expected, since substitution of Eq. (2) and $\rho_{xx}=(wt/l)V_x/I$ into Eq. (5) yields Eq. (4). The only difference is the ohmic assumption, $R_x=V_x/I$, which holds very well in these films. The continuous curves are, in effect, empirical fits of Eq. (5) to the data. It is also interesting to plot the Hall mobility μ_H, obtained directly from

$$\mu_H=1/(B\cot\theta_H)\ . \tag{6}$$

Figure 7 shows plots of the Hall mobility versus temperature for samples Nos. 1–5. Also shown are μ_H values for single crystal YBCO with $x\approx 7$ reproduced from Carrington *et al.*[30] The Hall mobility rises as the temperature decreases and then drops sharply at the transition temperature. For a given temperature, μ_H also increases as x increases with our sample No. 4 having a mobility

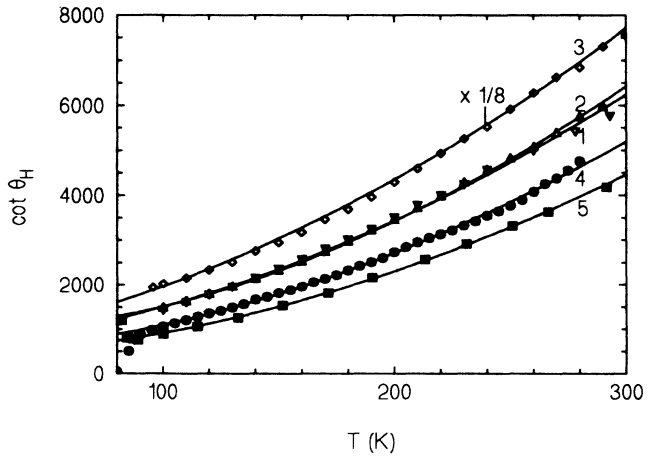

FIG. 6. Variation of the inverse Hall angle, $\cot\theta_H$, with temperature for a number of samples. Note that for sample No. 3 $\cot\theta_H$ is $\times\frac{1}{8}$. The continuous curves are empirical fits from Eq. (5).

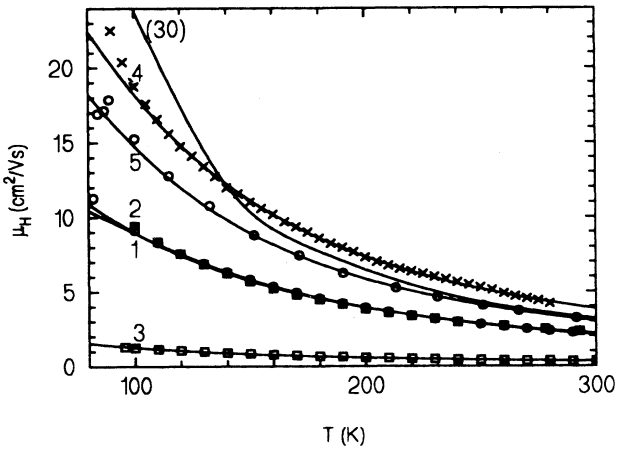

FIG. 7. Hall mobility μ_H vs temperature. The continuous curves are empirical fits using Eq. (6). The continuous unmarked curve (30) is single-crystal $YBa_2Cu_3O_7$ data from Ref. 30.

similar to the bulk crystal. However, in our as-grown films μ_H increases as x increases, whereas the reverse occurs for the *ex situ* process.

The continuous curves in Fig. 6 are empirical fits obtained by substituting Eqs. (1) and (3) into (5), which yields

$$\cot\theta_H=[(C/R_{H0}+B\alpha)+(C\alpha+A/R_{H0})T +(B/R_{H0})/T+A\alpha T^2]/B_z\ . \tag{7}$$

Effective carrier relaxation times τ_H and mobilities are given by $\cot\theta_H=1/(\omega_c\tau_H)$, where $\omega_c=(e/m^*)B_z$ is the cyclotron resonant frequency and m^* the effective mass. The components of τ_H and μ_H are then obtained from Eq. (7):

$$\tau_1=(m^*/e)\mu_1,\quad \text{where } \mu_1=(C/R_{H0}+B\alpha)^{-1}\ , \tag{8a}$$

$$\tau_2=(m^*/e)\mu_2,\quad \text{where } \mu_2=(C\alpha+A/R_{H0})^{-1}T^{-1} \tag{8b}$$

$$\tau_3=(m^*/e)\mu_3,\quad \text{where } \mu_3=(B/R_{H0})^{-1}T \tag{8c}$$

$$\tau_4=(m^*/e)\mu_4,\quad \text{where } \mu_4=(A\alpha T)^{-2}\ . \tag{8d}$$

Calculated values of the room-temperature mobility components are listed in Table II, which also lists the total effective mobility μ_H calculated from

$$1/\mu_H=1/\mu_1+1/\mu_2+1/\mu_3+1/\mu_4\ .$$

The temperature dependencies of the mobility components may be compared with the scattering mechanisms listed in Table III. The strongest effect arises from the T^{-2} term, which also gives rise to the approximate square-law temperature dependence of $\cot\theta_H$ shown in Fig. 8 and given by

$$\cot\theta_H=A_H+B_HT^2\ , \tag{9}$$

where values of the coefficients A_H and B_H are recorded in Table II.

TABLE II. Coefficients for $\cot\theta_H$, Eq. (9), oxygen content x, room-temperature mobility components $\mu_1-\mu_4$, and effective mobility μ_H.

Device No.	$\cot\theta_H$		x	Mobility components at 300 K ($cm^2 V^{-1} s^{-1}$)				
	B_H (10^{-2} K^{-2})	A_H (10^3)		μ_1 (T^0)	μ_2 (T^{-1})	μ_3 (T^1)	μ_4 (T^{-2})	μ_H
3. Y78MP	7.14	1.362	6.5	4.99	1.91	248.4	0.58	0.41
2. Y113MP	6.14	0.945	6.7	158.1	6.45	106.0	2.97	1.97
1. Y111MP	5.84	1.053	6.72	66.19	6.76	256.7	3.56	2.23
5. Y84MP	4.36	0.538	6.8	128.8	12.87	340.2	4.06	2.99
4. Y116SP	5.20	0.604	6.85	190.8	14.33	396.7	5.37	3.79

IV. DISCUSSION

The temperature dependence of the longitudinal resistivity and Hall effect of as-grown c-axis-oriented YBCO films are generally similar to films prepared by *ex situ* oxidation processes. The $R-T$ and $1/R_H-T$ characteristics are nearly linear, and $\cot\theta_H \propto T^2$. Small deviations from these laws have been investigated in this paper and a quadratic fit obtained for the resistivity data [Eq. (1)] and a cubic fit for $\cot\theta_H$ [Eq. (7)] data, but with linear and quadratic terms dominating, respectively. By substituting these empirical expressions for the resistivity and Hall coefficient into $\cot\theta_H$, expressions for the effective carrier relaxation times and mobilities [Eq. (8)] were obtained. It is emphasized that these are empirical and effective values. We can, however, compare the effective mobility components in Eq. (8) with various scattering mechanisms as indicated in Table III. Scattering due to neutral impurities appears weak, except in sample No. 3 of Table II. In this sample a relatively large value of residual resistance also occurs as indicated by the value of C in Table I. The T^{-1} scattering term is strong in all the samples, but the overall mobility is limited by the T^{-2} term. A number of different models have been proposed to explain the Hall-effect results.[7,8,39–43] Of these, probably Anderson's theory based on a Luttinger liquid[43] has received the most recent attention. In this the inverse Hall angle is given by Eq. (9), where $A_H=0$ in a pure sample, A_H is proportional to Ni and Zn doping in YBCO and B_H is constant for all dopings. In our samples the slope of $\cot\theta_H$, B_H is fairly constant with x and has a mean value of 5.74×10^{-2} K^{-2} (Table II). A_H decreases by about one half as x increases from 6.5 to 6.85. Any further detailed comparison of these results with theory is probably inappropriate, since we find that the mobility and inverse Hall angle vary differently with oxygen compared with other work. Figure 9 shows a plot of mobility versus oxygen content x for our *in situ* results. Also shown are three sets of results obtained from *ex situ* oxidized YBCO c-axis films on $LaAlO_3$ by laser ablation or a BaF_2 process (29), laser ablation of YBCO on $SrTiO_3$ (30), and off-axis dc sputtering of YBCO on MgO (100) (31). Also shown is one set of results for bulk polycrystalline YBCO (19). In this comparison we used $\mu_H=1/(B\cot\theta_H)$ to convert $\cot\theta_H$ data in the references to μ_H using Fig. 1(b) at 250 K from (29), Fig. 9 at 300 K from (30), Fig. 4 at 300 K from (31), and data at 200 K from (19). In comparing the thin-film results the mismatch between film and substrates is a source of lattice defects. However, the mobility results for films on $SrTiO_3$ (100) and MgO (100) are similar for the *ex situ* oxidation even though the mismatches between these two substrates are 2% and 9%, respectively. There is also a

TABLE III. Possible scattering mechanisms for the mobility (or relaxation time) temperature dependencies as determined from Eqs. (7) and (8).

Possible scattering mechanism	Mobility temperature dependence	Measured
(1) Neutral impurity, spinon-magnetic impurity	T^0	Weak except μ_1 in sample No. 3 (Table II)
(2) Hole-phonon, holon-spinon, boson-phonon, boson-impurity	T^{-1}	Strong in μ_2
(3) Dislocation	T^1	Weak in μ_3
(4) Electron-hole, spinon-spinon, boson-boson	T^{-2}	Very strong in μ_4
(5) Acoustic phonon	$T^{-1.5}$	None
(6) Charged impurity	$T^{1.5}$	None

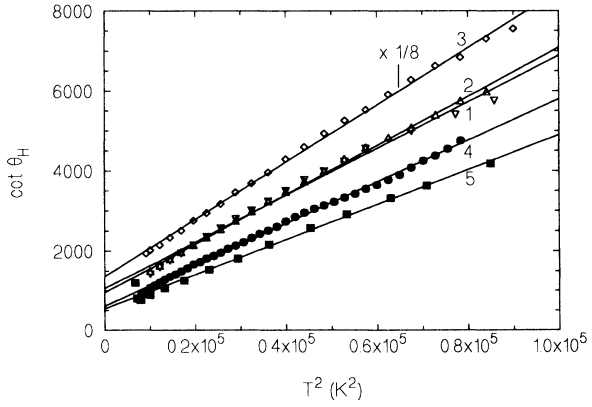

FIG. 8. $\cot\theta_H$ plotted as a function of T^2. The continuous lines are fits to the equation $\cot\theta_H=A_H+B_HT^2$, where values of the coefficients A_H and B_H are recorded in Table II.

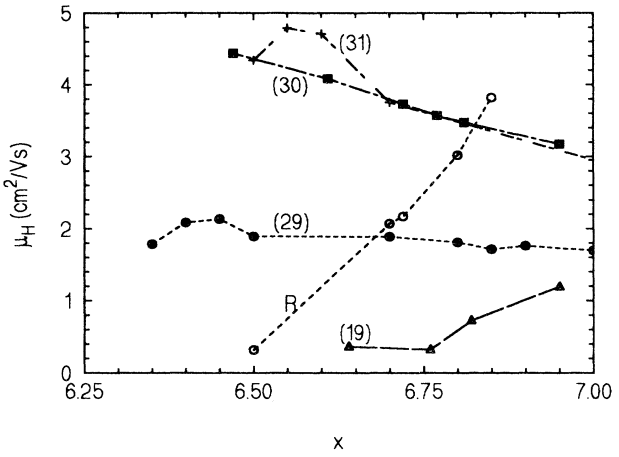

FIG. 9. Comparison of the Hall mobility μ_H with oxygen content x for this paper (R) and c-axis oriented $YBa_2Cu_3O_x$ films, Refs. 29, 30, and 31, and bulk polycrystalline $YBa_2Cu_3O_x$ Ref. 19.

large difference between our *in situ* oxidized results for growth on MgO (100) compared with the *ex situ* results for MgO (100) and $SrTiO_3$ (100), which suggests that the results are not strongly dependent on these substrates. The comparison with $LaAlO_3$ results may not be so clear because of the heavy twinning, which occurs in films grown on these substrates. Generally, in the *ex situ* process μ_H decreases slightly or is nearly constant with increasing x. In the *in situ* case μ_H increases sharply with increasing x. A rather smaller increase occurs for the bulk YBCO example. The opposite is true of course for $\cot\theta_H$, which increases with oxygen for the *ex situ* case and also for impurity Zn and Fe doping in single-crystal $YBa_2Cu_{3-x}Zn_xO_{7-\delta}$ (Ref. 24) and $YBa_2Cu_{3-x}Fe_xO_{7-\delta}$ (Ref. 25). A possible explanation is that the oxidation mechanisms are different in the two processes. In the *in situ* process the final oxidation takes place immediately after growth as the film cools in the surrounding oxygen gas, during which the film structure changes from tetragonal to orthorhombic. The *ex situ* process involves taking a fully oxygenated film, after growth and converting it to the required stoichiometry by heating in oxygen. The result is that in the *in situ* process the mobility increases and scattering decreases with increasing oxygen constant, whereas the opposite occurs for films prepared by the *ex situ* process. This suggests that the two oxidation processes lead to different lattice defects in these nonstoichiometric compounds. This could be elucidated further by a detailed investigation of the energy of formation and distribution of the lattice defects.

V. CONCLUSIONS

In this paper we have reported measurements of the temperature dependence of the resistivity and Hall coefficient of *in situ*—prepared $YBa_2Cu_3O_x$ thin films. The resulting data was used to formulate expressions for the inverse Hall angle $-\cot\theta_H$ and effective mobility μ_H. In these expressions quadratic-temperature-dependent terms dominated, as for *ex situ*—oxidized films, and we account for other terms as due to other possible scattering mechanisms. However, the Hall mobility μ_H increases sharply, and $\cot\theta_H$ decreases with increasing oxygen content, which is the opposite of that found in films reoxidized after growth. This anomaly is discussed in terms of the oxidation conditions for the two cases which lead to different lattice defects.

ACKNOWLEDGMENTS

We acknowledge support given by the Engineering and Physical Sciences Research Council (previously SERC) for part of this research. Also discussions with colleagues at the University of Cambridge Interdisciplinary Research Centre in Superconductivity, in particular, Dr. Jan Evetts and Dr. Rob Somekh on sputtering and Professor George Walmsley, Queens University, Belfast.

[1]Duan Hong-min, Lu Li, Wang Xie-mei, Lin Shu-yuan, and Zhang Dian-lin, Solid State Commun. **64**, 489 (1987).
[2]Z. Yong, Z. Qirui, K. Weiyan, X. Jansheng, H. Zhenhui, S. Shifang, C. Zuyao, Q. Yitai, P. Guoqiang, and W. Y. Kuan, Solid State Commun. **64**, 885 (1987).
[3]S. W. Tozer, A. W. Kleinsasser, T. Penney, D. Kaiser, and F. Holtzberg, Phys. Rev. Lett. **59**, 1768 (1987).
[4]T. Penney, S. von Molnár, D. Kaiser, F. Holtzberg, and A. W. Kleinsasser, Phys. Rev. B **38**, 2918 (1988).
[5]P. W. Anderson and Z. Zou, Phys. Rev. Lett. **60**, 132 (1987).
[6]P. W. Anderson, Science **256**, 1526 (1992).
[7]A. S. Alexandrov, A. M. Bratkovsky, and N. F. Mott, Supercond. Sci. Technol. **6**, 755 (1993).
[8]A. S. Alexandrov, A. M. Bratkovsky, and N. F. Mott, Phys. Rev. Lett. **72**, 1734 (1994).
[9]A. J. Scholfield and J. M. Wheatley, Phys. Rev. B **47**, 11 607 (1993).
[10]B. W. Ricketts, R. B. Roberts, R. Driver, and H. K. Welsh, Solid State Commun. **64**, 1287 (1987).
[11]L. Forró, M. Petravić, and B. Leontić, Solid State Commun. **65**, 1355 (1988).
[12]M. Galffy and E. Zirngiebl, Solid State Commun. **68**, 929 (1988).
[13]A. M. Ghorayeb, O. Gorochov, D. M. Eagles, M. Rateau, R. Suryanarayanan, and H. Pankowska, Physica C **153-155**, 1363 (1988).
[14]M. Affronte, J. Y. Genoud, T. Graf, M. Decroux, and O. Fischer, Phys. Rev. B **45**, 8189 (1992).
[15]H. Zhenhui, Z. Han, S. Shifang, C. Zuyao, Z. Qirui, and X. Jiansheng, Solid State Commun. **66**, 1215 (1988).
[16]M. Affronte, D. Pavuna, M. Francois, F. Licci, T. Basagni, and S. Cattani, Physica C **162-164**, 1007 (1989).
[17]G. Ilonca, M. Mehbod, A. Lanckbeen, and R. Deltour, Phys. Rev. B **47**, 15 265 (1993).
[18]G. Priftis, A. M. Ghorayeb, O. Gorochov, R. Suryanarayanan, H. Pankowska, and M. Rateau, Physica C **162-164**, 1201 (1989).
[19]G. Kallias, I. Panagiotopoulos, D. Niarchos, and A. Kostikas,

Phys. Rev. B **48**, 15 992 (1993).
[20]N. Thier and K. Winzer, IEEE Trans. Magn. **MAG-25**, 2293 (1989).
[21]L. Forró and A. Hamzic, Solid State Commun. **71**, 1099 (1989).
[22]M. Affronte, M. Decroux, W. Sadowski, T. Graf, and O. Fischer, Physica C **172**, 131 (1990).
[23]J. P. Rice, J. Giapintzakis, D. M. Ginsberg, and J. M. Mochel, Physica C **185**, 1853 (1991).
[24]T. R. Chien, Z. Z. Wang, and N. P. Ong, Phys. Rev. Lett. **67**, 2088 (1991).
[25]M. D. Lan, J. Z. Liu, Y. X. Jia, Lu Zhang, and R. N. Shelton, Phys. Rev. B **49**, 580 (1994).
[26]H. L. Stormer, A. F. J. Levi, K. W. Baldwin, M. Anzlowar, and G. S. Boebinger, Phys. Rev. B **38**, 2472 (1988).
[27]Y. Iye, S. Nakamura, and T. Tamegai, Physica C **159**, 616 (1989).
[28]R. Hopfengartner, M. Leghissa, G. Kreiselmeyer, B. Holzapfel, P. Schmitt, and G. Seamann-Ischenko, Phys. Rev. B **47**, 5992 (1993).
[29]E. C. Jones, D. K. Christen, J. R. Thompson, R. Feenstra, S. Zhu, D. H. Lowndes, J. M. Phillips, M. P. Siegal, J. D. Budai, Phys. Rev. B **47**, 8986 (1993).
[30]A. Carrington, D. J. C. Walker, A. P. Mackenzie, and J. R. Cooper, Phys. Rev. B **48**, 13 051 (1993).
[31]B. Wuyts, E. Osquiguil, M. Maenhoudt, S. Libbrecht, Z. X. Gao, and Y. Bruynseraede, Physica C **222**, 341 (1994).
[32]M. S. Raven, E. E. Inameti, W. M. Wan, and B. G. Murray, Supercond. Sci. Technol. **7**, 462 (1994).
[33]M. S. Raven, J. Mater. Sci. Mater. Electron. **5**, 129 (1994).
[34]E. E. Inameti, M. S. Raven, W. M. Wan, and B. G. Murray, Vacuum **43**, 121 (1992).
[35]J. D. Jorgensen, B. W. Veal, A. P. Paulikas, L. J. Nowicki, G. W. Crabtree, H. Claus, and W. K. Kwok, Phys. Rev. B **41**, 1863 (1990).
[36]Y. M. Wan, Ph.D. thesis, University of Nottingham, 1993.
[37]M. Gurvitch and A. T. Fiory, Appl. Phys. Lett. **51**, 1027 (1987).
[38]P. Blood and J. W. Orton, *The Electrical Characterization of Semiconductors: Majority Carriers and Electron States* (Academic, London, 1992), p. 15.
[39]D. Y. Xing and C. S. Ting, Phys. Rev. B **38**, 5134 (1988).
[40]A. Davidson, P. Santhanam, A. Palevski, and M. J. Bray, Phys. Rev. B **38**, 2828 (1988).
[41]D. X. Xing, Z. D. Wang, and C. D. Gong, Z. Phys. B **77**, 61 (1989).
[42]D. M. Eagles and N. Savvides, Physica C **158**, 258 (1989).
[43]P. W. Anderson, Phys. Rev. B **67**, 2092 (1991).